

GALACTIC COSMIC RAYS—CLOUDS EFFECT AND BIFURCATION MODEL OF EARTH GLOBAL CLIMATE

V.D. Rusov^{1,2}

¹ *National Polytechnical University, Odessa, Ukraine*

² *Bielefeld University, Bielefeld, Germany*

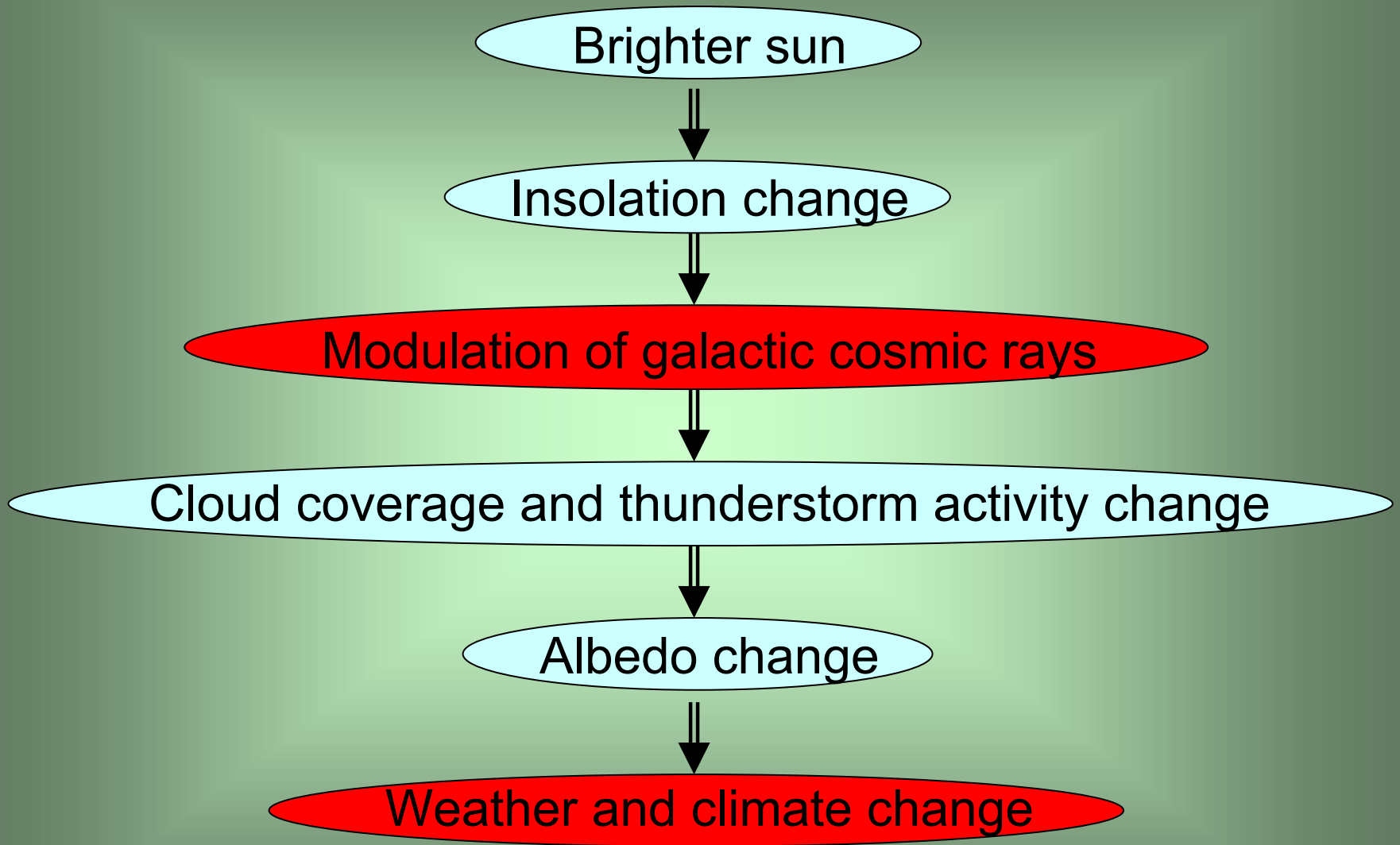


Fig.3. Magnetic reconnection

[Holmon G.D., Scientific American, 2005]

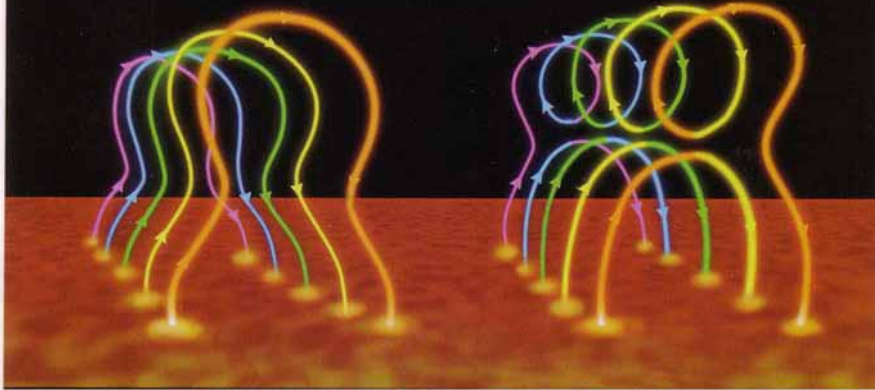
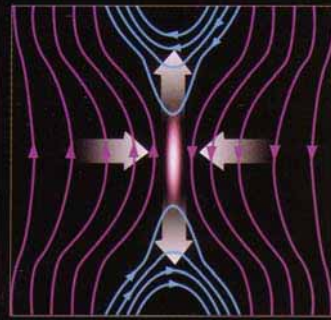
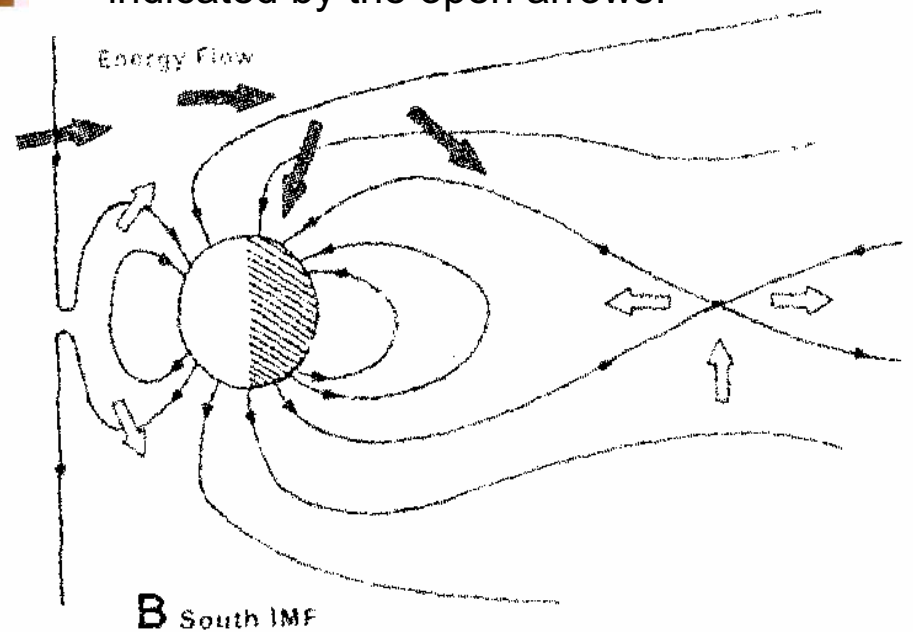
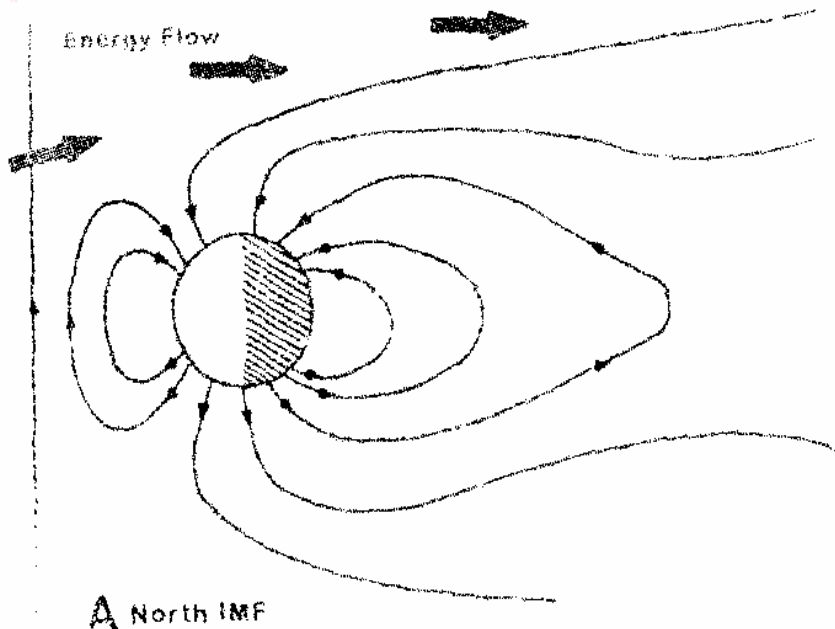


Fig.4. Schematic of the process of magnetic reconnection [Lyon J.G. Nature, 2000].

- A. No reconnection and no energy flow into the magnetosphere. Energy flow is indicated by solid arrows.
- B. Reconnection opens the magnetosphere and allows entry of plasma, momentum and energy. Magnetosphere convection is indicated by the open arrows.



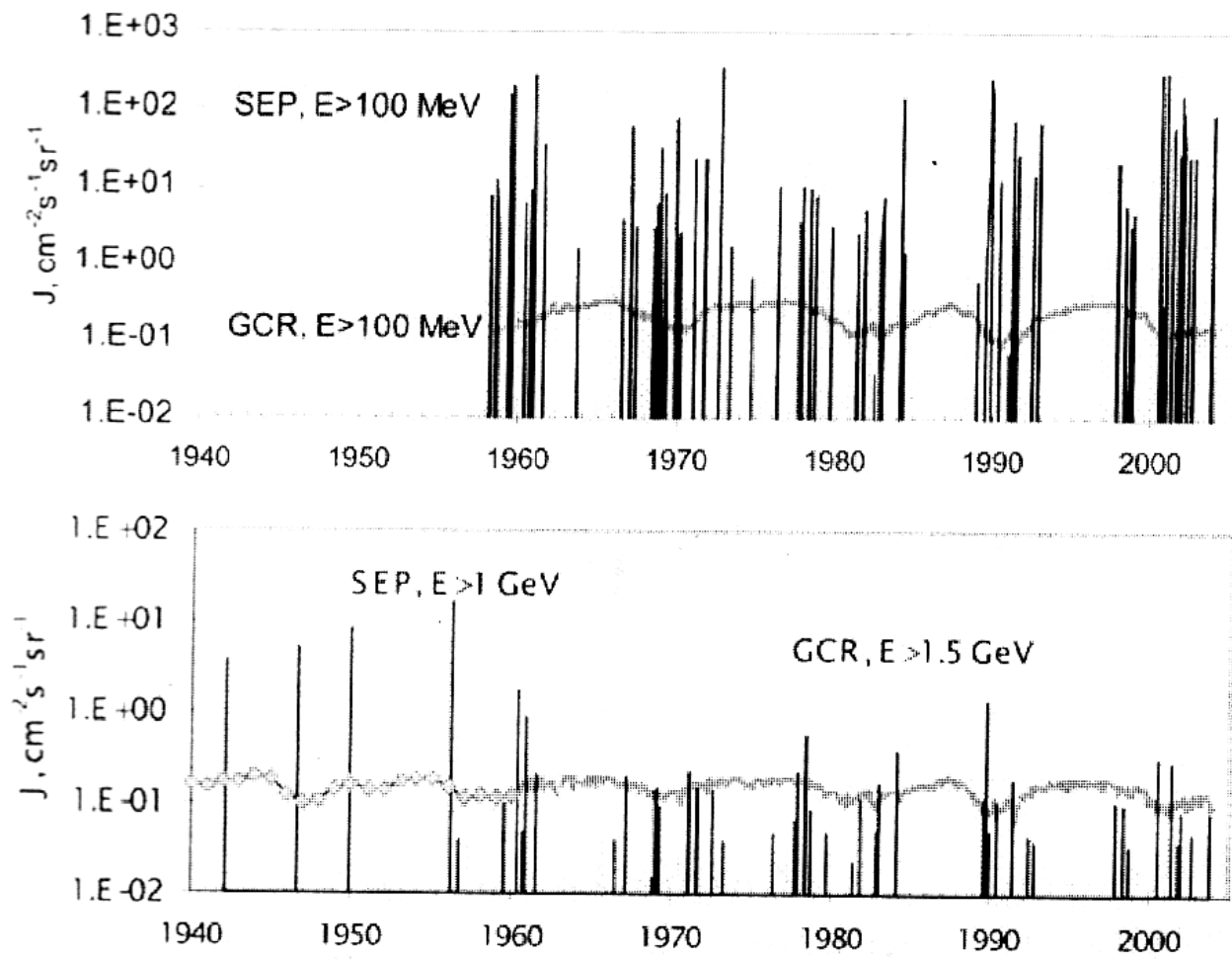


Fig.5. The data by Bazilevskaya [Advanced in Space Research, 2004] illustrate the explicit and exact example of inverse correlation between the GCR intensity with energy above 1.5 GeV and the solar activity (protons with energy above 1.0 GeV) on the basis of the LPI balloon observations during the 1958-2002 years.

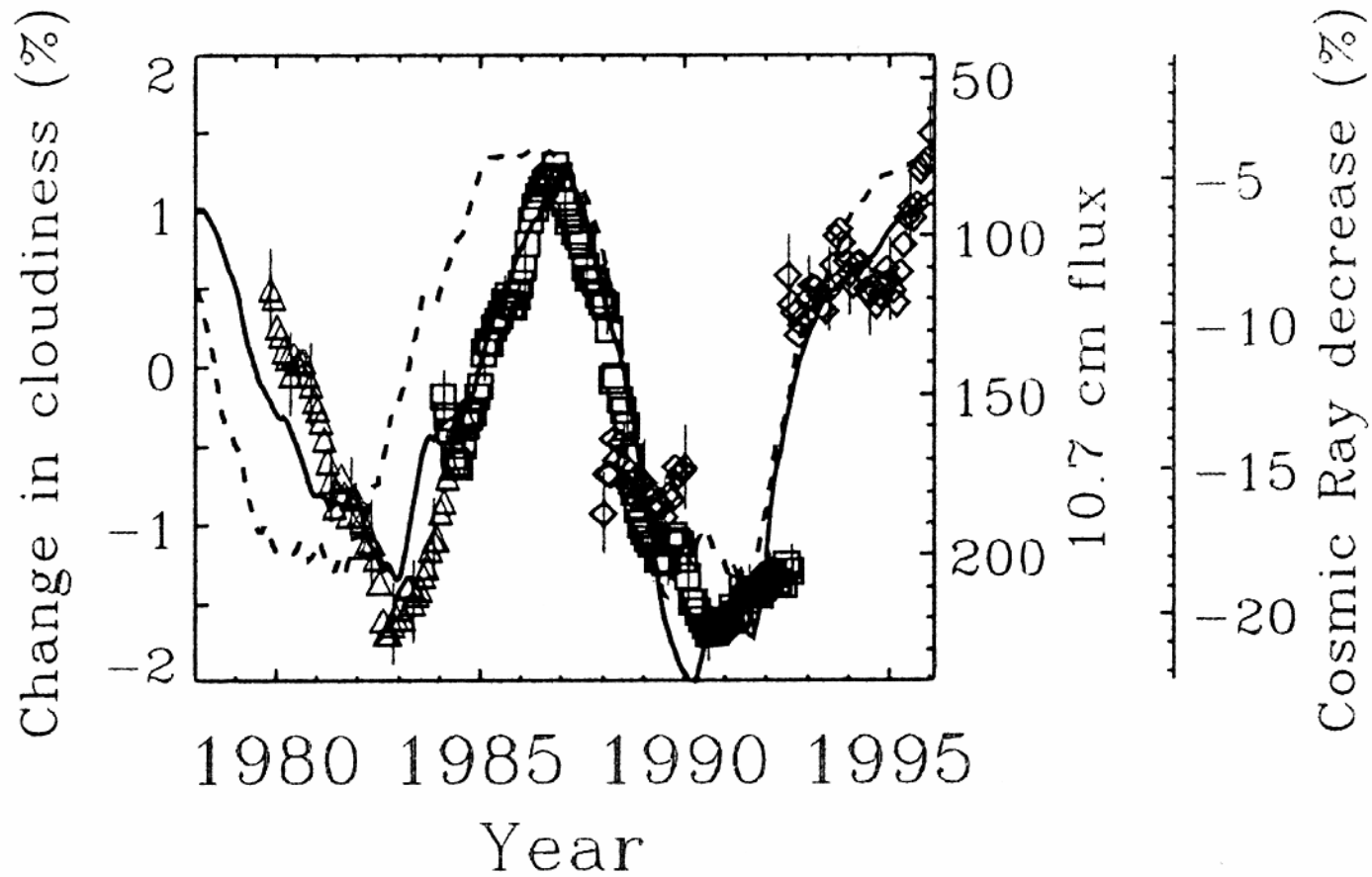


Fig.6. Data by Svensmark and Friis-Christensen [*J. Atmos. Sol.-Terr. Phys.*, 1997] demonstrate the high positive correlation of galactic CRF and cloudiness during long-term cosmic ray modulation in the 11-year solar activity cycle.

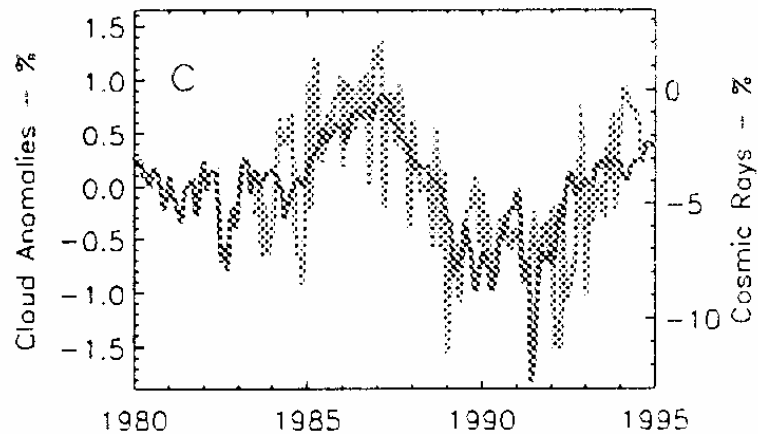
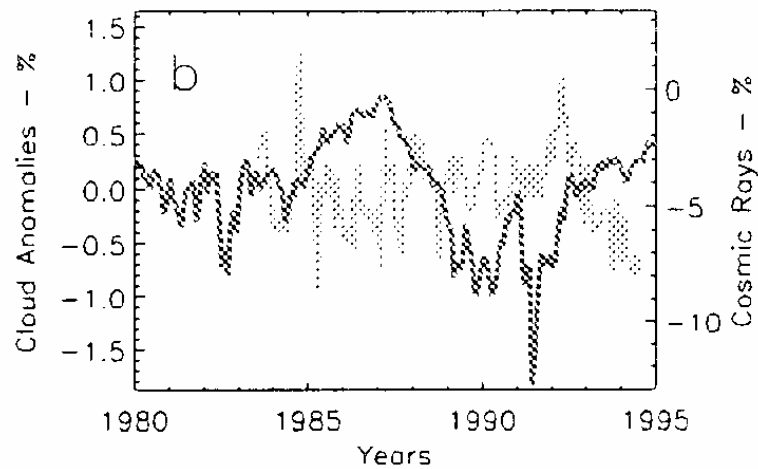
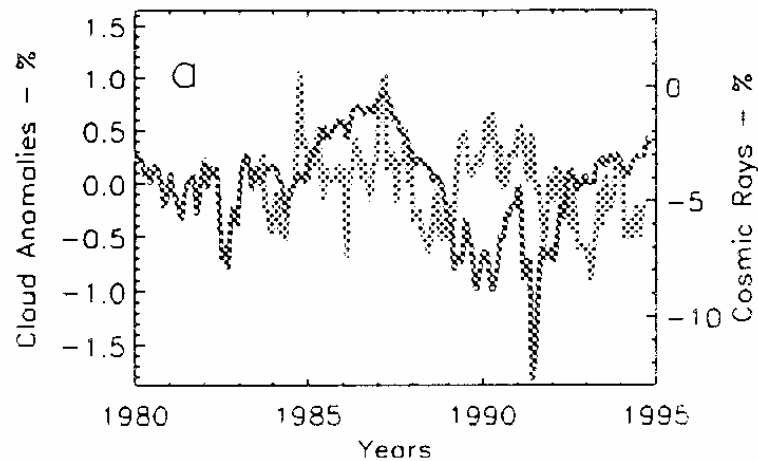


Fig.7. [Marsh and Svensmark, Phys. Rev. Lett., 2000]. Global average of monthly cloud anomalies for (a) high (<440 hPa), (b) middle (440 – 680 hPa) and (c) low (>680 hPa) cloud cover. The cosmic rays represent neutron counts observed at Huancayo (cutoff rigidity 12.91 GeV) and normalized to October 1965.

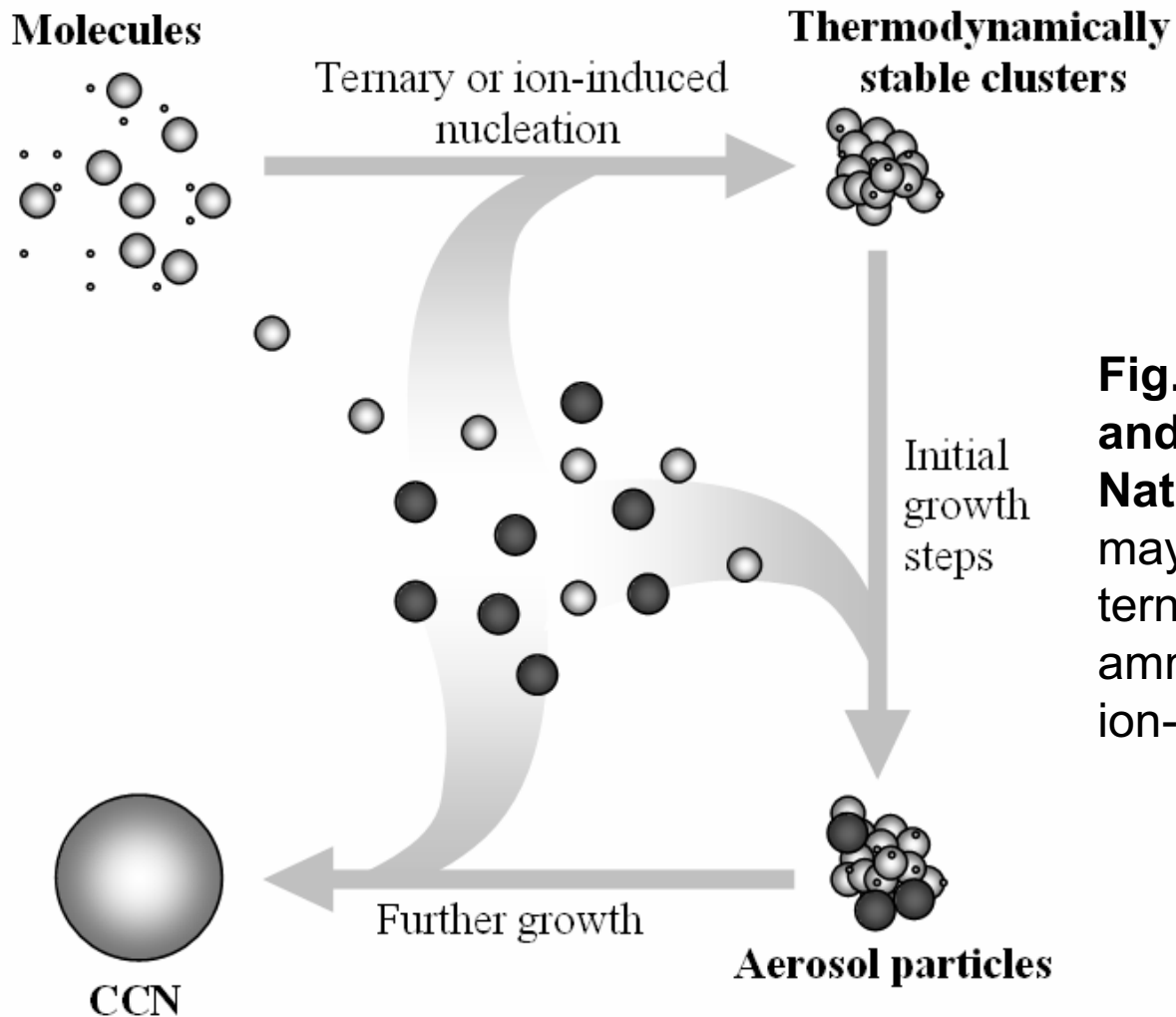


Fig.8. How particles form and grow [Kulmala M., Nature, 2003]: Nucleation may involve homogeneous ternary water-sulfuric acid-ammonia mixture or may be ion-induced.

The initial steps of growth include activation of inorganic clusters by soluble organic molecules, heterogeneous nucleation of insoluble organic vapors on inorganic clusters, and chemical reactions of organic molecules at surfaces of inorganic clusters. Finally, cloud condensation nuclei (CCN) form through addition of organic and sulfuric acid molecules.

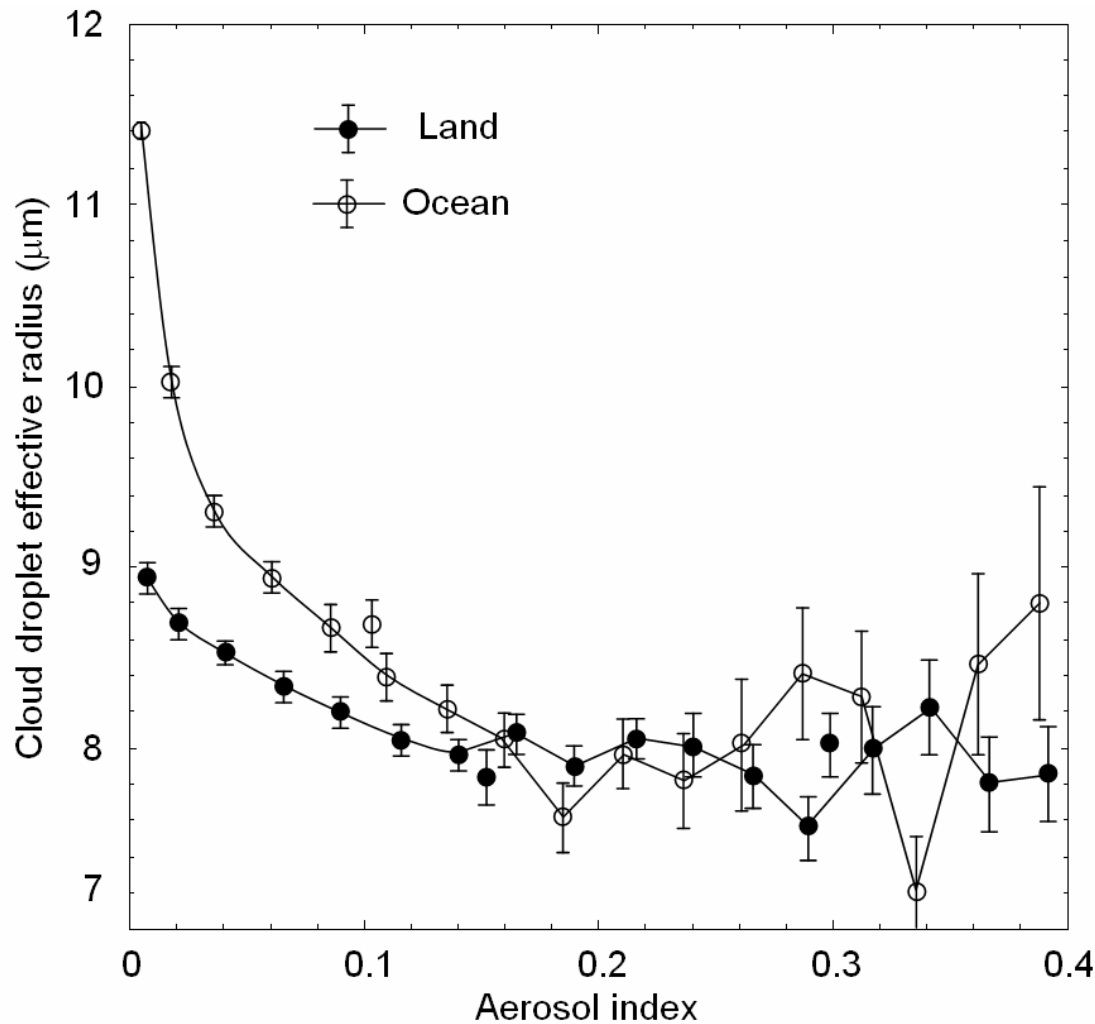


Fig.9. Effect of aerosol on cloud droplet: mean cloud droplet effective radius (CDR) as a function of aerosol load [*Breon et al., Science 2002*]. The two curves show the mean CDR as a function of aerosol index (AI) for land (lower curve) and ocean (upper curve).

On possible relation between cosmic rays-cloud and indirect aerosol effects

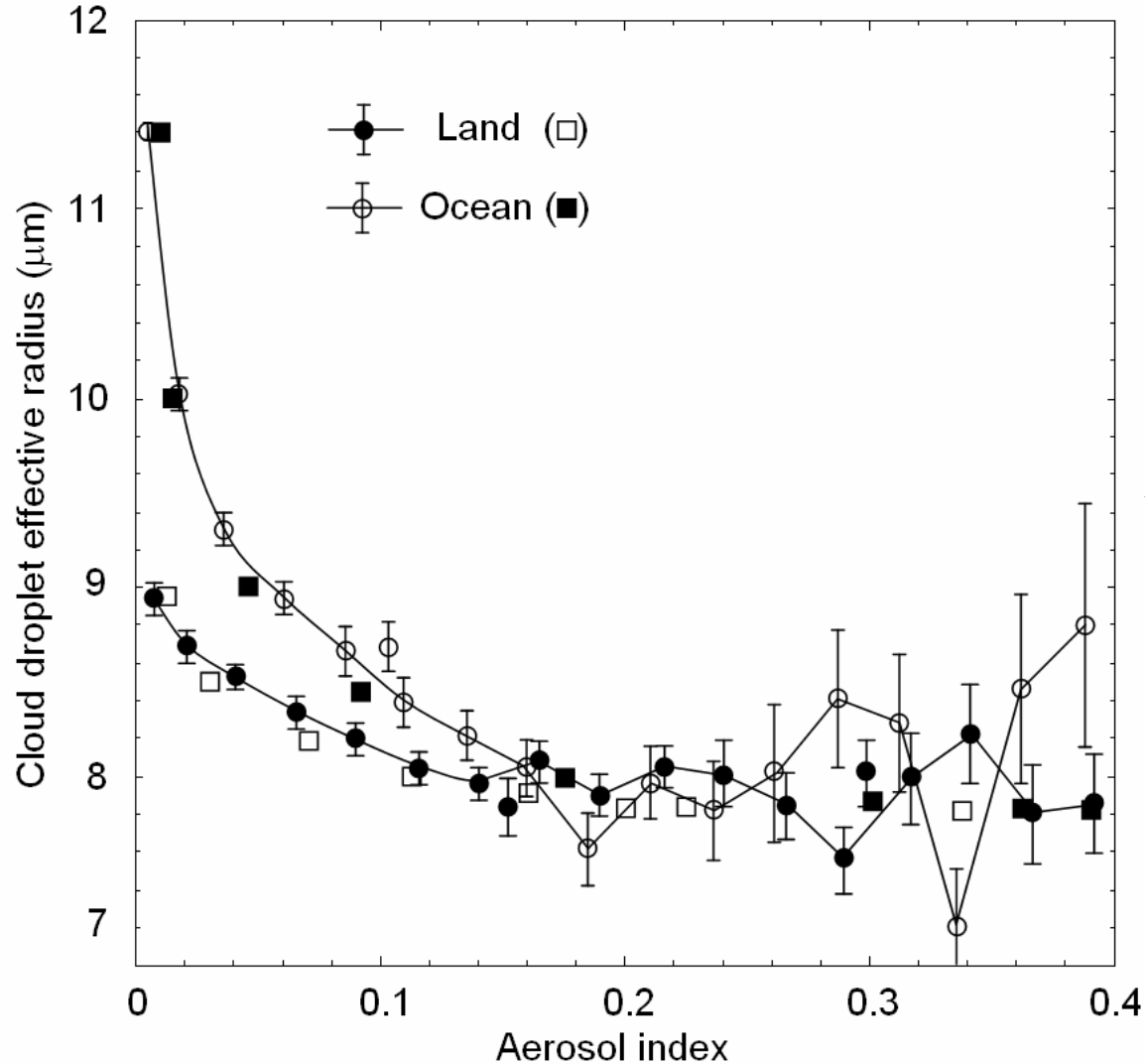


Fig.9b. Effect of aerosol on cloud droplet.

$$AI = \left[\frac{1}{(0.6r_{eff} - 4.385)r_{eff}} - \frac{\eta}{r_{eff}} \right]^{1.429}$$

$$\eta = \begin{cases} 0, & \text{over ocean,} \\ 0.63, & \text{over land,} \end{cases} \quad (1)$$

where $r_{eff} = \langle r^3 \rangle / \langle r^2 \rangle$ is the mean CDR, and r is the radius of the cloud droplets

$$N_d \approx (N_{CCN})^\alpha \quad (2)$$

$$N_d \approx \frac{1}{(0.6r_{eff} - 4.385)r_{eff}} - \frac{\eta}{r_{eff}} \quad (3)$$

$$\langle V_w \rangle_{ocean,land} = p_i V_{atm} \cdot \frac{4}{3} \pi \langle r \rangle^3 N_d = p_i V_{atm} \cdot \frac{4\pi}{3} \frac{r_{eff}^2}{k_r^3} \left(\frac{1}{0.6r_{eff} - 4.385} - \eta \right), \quad (4)$$

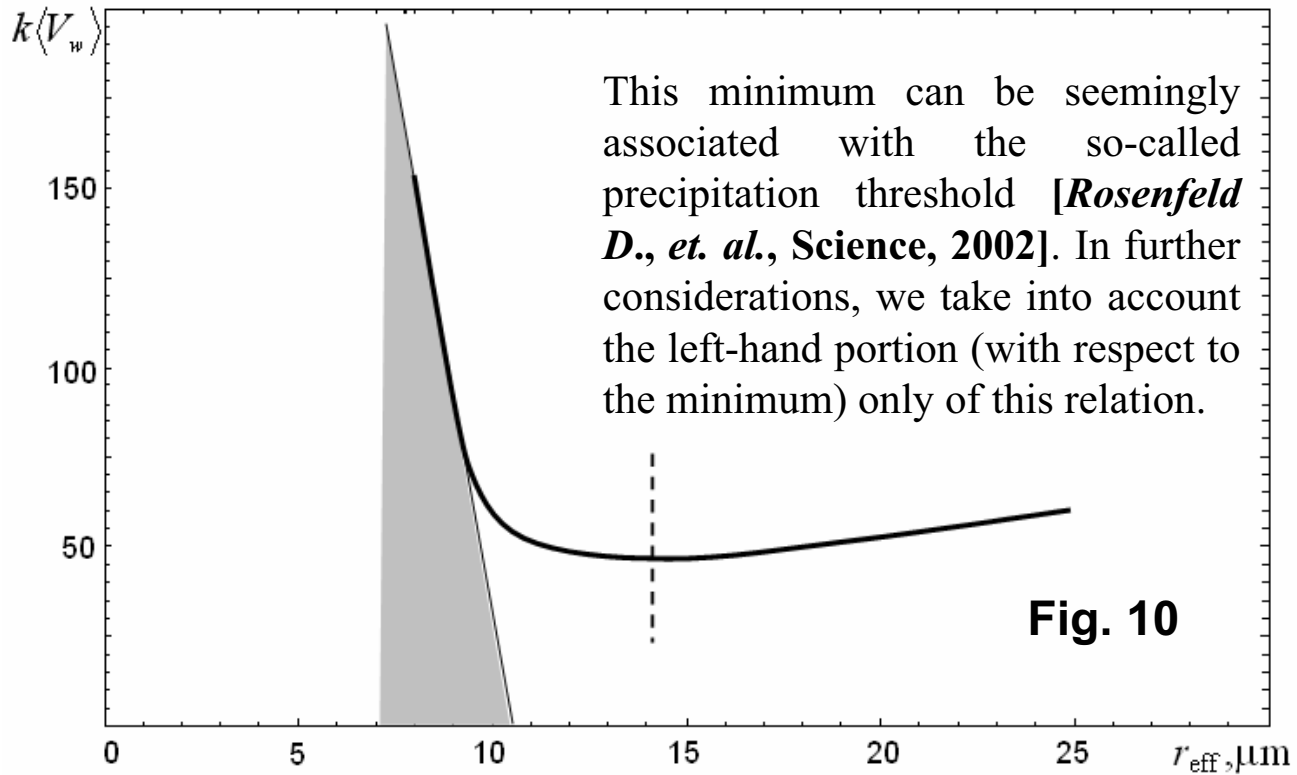
where $V_{atm} \cong const$ is the total volume of the atmosphere, p_i is the portion of the atmosphere volume "over the ocean" or "over the land", $\langle r \rangle \approx k_r \cdot r_{eff}$ is the mean radius of cloud droplets.

$$\langle V_w \rangle = V_{atm} \cdot \frac{4\pi}{3} \frac{r_{eff}^2}{k_r^3} \left[\frac{1}{0.6r_{eff} - 4.385} - \frac{S_{land} \Lambda}{S_{ocean} + S_{land}} 0.63 \right], \quad (5)$$

$$\Lambda = \Lambda(r_{eff} - 7.7) - \Lambda(r_{eff} - 9.6),$$

$$\Lambda(x) = \int_{-\infty}^x \delta(z) dz = \begin{cases} 1, & x \geq 0; \\ 0, & x < 0; \end{cases}$$

where S_{land} and S_{ocean} are the areas of land and oceans respectively; $S_{land} / (S_{land} + S_{ocean}) \cong 0.29$.



$$\langle V_w \rangle \approx k_w (a - br_{eff}) = a_w + b_w T, \quad (6)$$

since (on basis of known experiments [Rosenfeld D., et al., Science, 2002])

$$r_{eff} = a_r - b_r T_{cloud}. \quad (7)$$

Then total volume of liquid and vapor water in atmosphere:

$$\langle V_{w+v} \rangle \approx a_{wv} + b_{wv} T. \quad (8)$$

On the one hand, such an influence must be conditioned on the effect of inverse correlation between the magnitude of Φ_{GCR} and land temperature, T , which was experimentally ascertained by Svensmark [**Phys. Rev. Lett., 1998**]. This fact can be conditionally written as follows

$$\Phi_{GCR} \downarrow \uparrow \Rightarrow T \uparrow \downarrow, \quad (9)$$

where the arrows " \uparrow " and " \downarrow " show the increase and decrease of physical quantity respectively.

On the other hand, известно (on basis of known experiments [**Rosenfeld D., et. al., Science, 2002**]), что

$$r_{eff} = a_r - b_r T_{cloud}. \quad (7)$$

Hereinafter, taking into account the Eddington approximation for the outer boundary of atmosphere, we suppose that $T_{cloud} \sim const \cdot T$. Then, subject to Eqs. (7) and (1), the following conditional dependence can be written

$$T \uparrow \downarrow \Rightarrow r_{eff} \downarrow \uparrow \Rightarrow AI \uparrow \downarrow. \quad (10)$$

At last, by virtue of dependences (7)-(9)-(10)

$$AI \uparrow \downarrow \Rightarrow \Phi_{GCR} \downarrow \uparrow$$

We can suppose that it is possible to take into account the additional influence of GCR intensity variation Φ_{GCR} in the atmosphere on aerosol index (AI) distribution as additional variation of total volume $\langle V_{w+v} \rangle$, which was obtained by Eq. (1):

$$\langle V_{w+v} \rangle \approx (a_{wv} + b_{wv}T) = (a_{wv} + b_{wv}T)k \frac{M}{M_0} = (a_{wv} + b_{wv}T)kM_{\oplus}^* \quad (11)$$

where following approximate equations are using:

$$k \frac{M}{M_0} \approx \frac{\Phi}{\Phi_0} . \quad (12)$$

Here M_{\oplus}^* is relatively geomagnetic paleointensity, which measured for past 2.25 million years [*Yamasaki T. and Oda H., Science, 2002*], Φ_0 and M_0 are cosmic rays flux and Earth's magnetic field measured, for example, in October 1965. [*Svensmark H., Phys. Rev. Lett., 1998*].

Catastrophe theory and energy-balance model of global climate

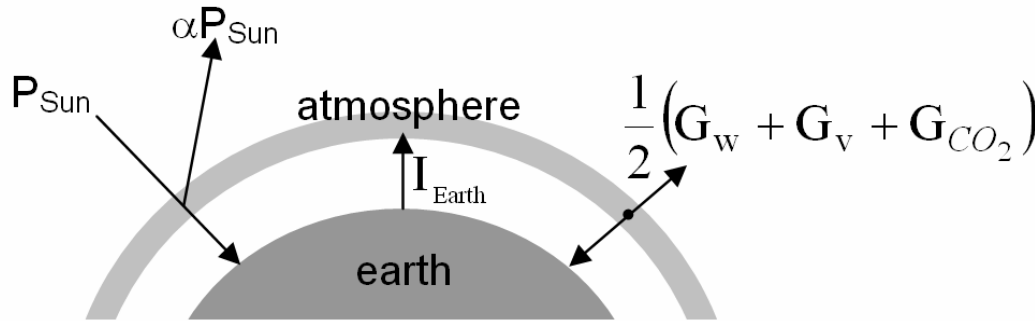


Fig.11. Balance of the absorbed and emitted energy currents on the surface of the Earth. With the purpose of simplification, we not consider other greenhouse gases.

Since the radiant equilibrium can be achieved at time scales of 10^4 years, the inclusion of greenhouse effect results in the following energy-balance equations for the ECS (see also Fig. 11)

$$U(T, t) = P_{Sun}(t) \cdot [1 - \alpha(T)] - I_{Earth}(T) + \frac{1}{2} G_w(T, t) + \frac{1}{2} G_v(T, t) + \frac{1}{2} G_{CO_2}(T, t), \quad (14)$$

where the first member of equations $U(T, t)$, if it not equals to zero, describes a magnitude of so-called "inertial" rate of heat variations in the ECS; $P_{Sun}(t) = (1/4)S(t) \cdot \gamma$ is the heat flow of solar radiation at the top of atmosphere (W); $S(t)$ is the insolation (W/m^2); α is the albedo of ECS; $I_{Earth} = \gamma \delta (\sigma T^4)$, W; $\delta = 0.95$; σ is the Stephen-Boltzmann constant; T is the temperature of Earth's surface (K); γ is the area of atmosphere outer boundary (m^2); t is the time, for which the energy balance is considered.

It is obvious that **Eq. (11)** for mean total volume of liquid water in the atmosphere allows writing down the following relation for the rate of re-emission

$$G_w(T, t) = \varepsilon_w \rho_w \langle V_w \rangle, \quad (15)$$

where ε_w is the mean radiant power for the unit mass of liquid water, ρ_w is the density of liquid water.

$$G_w(T, t) = \frac{\gamma H}{\langle V_{atm} \rangle} \varepsilon_w \rho_w \langle V_w \rangle = \frac{\gamma H}{\langle V_{atm} \rangle} \rho_w (a_{w\varepsilon} T^2 + b_{w\varepsilon} T + c_{w\varepsilon}) M_{\oplus}^*. \quad (16)$$

The expression for the rate of heat energy re-emitted by the water vapour can be similarly derived:

$$G_v(T, t) = \frac{\gamma H}{\langle V_{atm} \rangle} \varepsilon_v \rho_v \langle V_v \rangle = \frac{\gamma H}{\langle V_{atm} \rangle} \rho_v (a_{v\varepsilon} T^2 + b_{v\varepsilon} T + c_{v\varepsilon}) M_{\oplus}^*, \quad (17)$$

where ε_v is the mean radiant power for the unit mass of water vapour, ρ_v is the density of water vapour.

To examine a question on the functional dependence for the rate of heat energy $G_{CO_2}(T, t)$ on the temperature of ECS, use the analysis of known experimental data on the variations of temperature and carbon dioxide content over the past 420 kyr from the Vostok ice core [**Petit et al., Nature, 1999**]. It is obvious that these data are highly linear correlated. Therefore, it can be supposed that the dependence for the rate of heat energy on the temperature of ECS is also linear

$$G_{CO_2}(T, t) \approx \frac{\gamma H}{\langle V_{atm} \rangle} (a_{CO_2} T + b_{CO_2}). \quad (18)$$

It must be added that the dependence for the effective value of albedo on the temperature of ECS is chosen as the continuous parameterization

$$\alpha = \alpha_0 - \eta_\alpha \cdot (T - 273). \quad (19)$$

Equation (19) represents well, for example, the behaviour of albedo (under $\alpha_0=0.7012$, $\eta_\alpha=0.0295 \text{ K}^{-1}$) in the temperature range of 282-290 K.

Finally, assembling all partial contributions of heat fluxes (16)-(18) and $I_{Earth} = \gamma\delta(\sigma T^4)$ into the final energy-balance expression (14), we derive

$$U^*(T, t) = \frac{1}{4}T^4 + \frac{1}{2}a(t) \cdot T^2 + b(t) \cdot T, \quad (20)$$

where

$$a(t) = -\frac{1}{4\delta\sigma} a_\mu M_\oplus^*(t), \quad (21)$$

$$b(t) = -\frac{\eta_\alpha}{32\delta\sigma} \left[S(t) + \frac{4}{\eta_\alpha} \beta + \frac{4}{\eta_\alpha} b_\mu M_\oplus^*(t) \right], \quad (22)$$

$$U^*(T, t) = \frac{1}{4\gamma\delta\sigma} \left[\frac{1}{4}(1 - \alpha_\alpha - 273\eta_\alpha)S(t) + \frac{1}{2}b_{CO_2} H / \langle V_{atm} \rangle + \frac{1}{2}c_\mu M_\oplus^* - U(T, t) \right], \quad (23)$$

$$\beta = a_{CO_2} H / \langle V_{atm} \rangle, \quad [W/m^2 K]$$

$$a_\mu = (\rho_w a_{w\varepsilon} + \rho_v a_{v\varepsilon}) H / \langle V_{atm} \rangle, \quad [W/m^2 K^2],$$

$$b_\mu = (\rho_w b_{w\varepsilon} + \rho_v b_{v\varepsilon}) H / \langle V_{atm} \rangle, \quad [W/m^2 K],$$

$$c_\mu = (\rho_w c_{w\varepsilon} + \rho_v c_{v\varepsilon}) H / \langle V_{atm} \rangle, \quad [W/m^2],$$

Let us remind that the normalized variations of insolation, $\Delta\hat{S}=(S-S_0)/\sigma_S$, with mean value $\langle\Delta\hat{S}\rangle=\mathbf{0}$ and dispersion $\sigma_{\Delta\hat{S}}^2=1$ is applied more often for the simulation of the ECS.

Deriving an equation in the form of Eq. (20) with respect to ΔT , the following expression for the increment of heat rate ΔU^* can be defined

$$\Delta U^*(\Delta T, t) = \frac{1}{4} \Delta T^4 + \frac{1}{2} \tilde{a}(t) \cdot \Delta T^2 + \tilde{b}(t) \cdot \Delta T, \quad (24)$$

where

$$\tilde{a}(t) = -\frac{37.6}{\sigma T_0^3} a_\mu M_\oplus^*(t) = -\tilde{a}_0 \cdot M_\oplus^*(t), \quad (25)$$

$$\begin{aligned} \tilde{b}(t) &= -\frac{4.7\eta_\alpha\sigma_S}{\sigma T_0^3} \left[\Delta\hat{S}(t) + \frac{1}{\sigma_S} \left(S_0 - \frac{32\delta\sigma T_0^3}{\eta_\alpha} \right) + \frac{4}{\eta_\alpha} \cdot \frac{\varepsilon_{CO_2}\beta}{\sigma_S} + \frac{4}{\eta_\alpha} \cdot \frac{2a_\mu T_0 + b_\mu}{\sigma_S} M_\oplus^*(t) \right] = \\ &= -\frac{4.7\eta_\alpha\sigma_S}{\sigma T_0^3} \left[\Delta\hat{S}(t) + \frac{4}{\eta_\alpha} \cdot \frac{\varepsilon_{CO_2}\beta}{\sigma_S} + \frac{4}{\eta_\alpha} \cdot \frac{2a_\mu T_0 + b_\mu}{\sigma_S} M_\oplus^*(t) \right] = \\ &= -\tilde{b}_0 \left[\Delta\hat{S}(t) + \frac{4}{\eta_\alpha} \cdot \Delta\mathfrak{R}_{CO_2} + \frac{4}{\eta_\alpha} \cdot \Delta\mathfrak{R}_{w+v} M_\oplus^*(t) \right], \quad (26) \end{aligned}$$

The canonical form of the variety of the fold catastrophe, which represents a set of points $(\Delta T, \tilde{a}, \tilde{b})$, satisfies the equation (see Fig. 6a):

$$\frac{d}{d(\Delta T)} \Delta U^*(\Delta T, t) = \Delta T^3 + \tilde{a}(t) \cdot \Delta T + \tilde{b}(t) = 0. \quad (28)$$

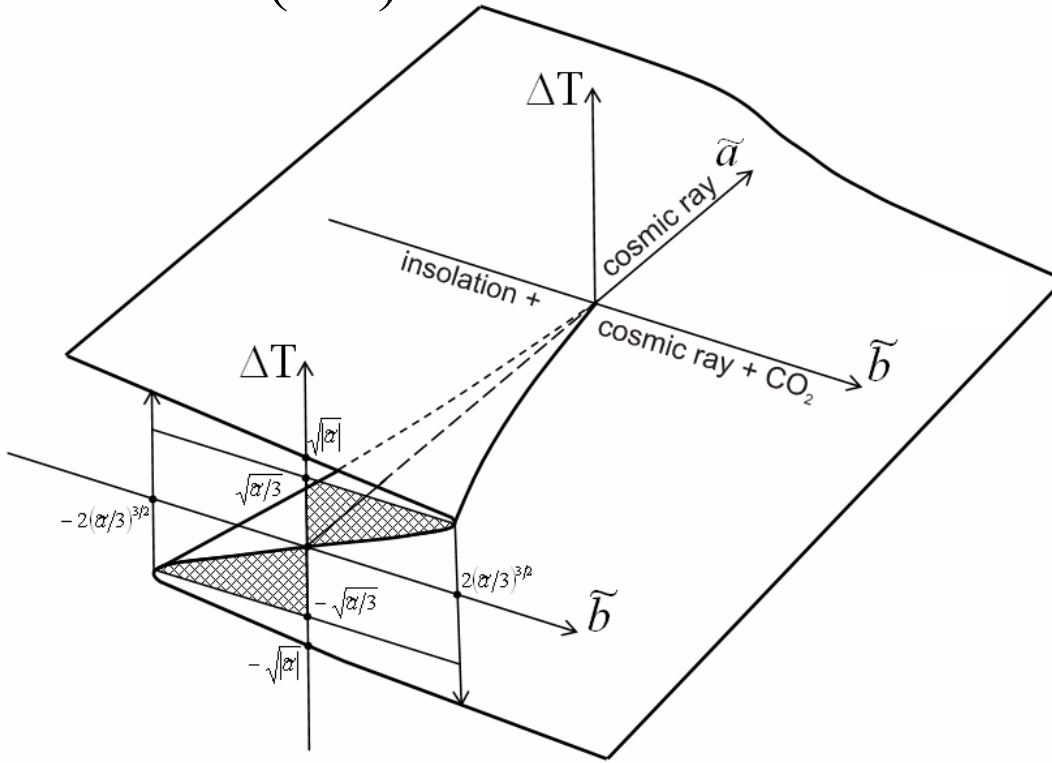


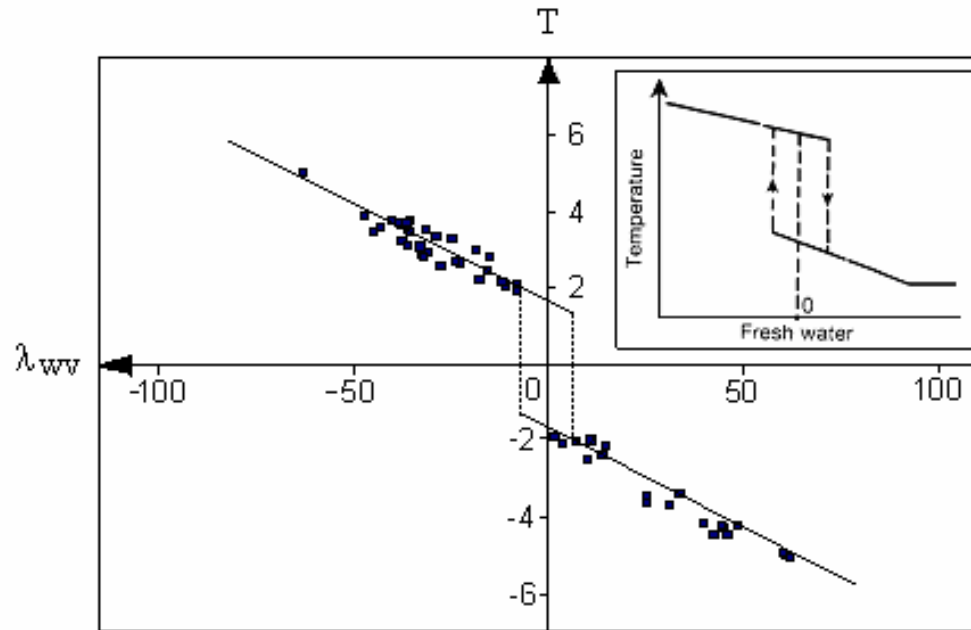
Fig.12. The canonical view of variety of the fold catastrophe as a set of points $(\Delta T, \tilde{a}, \tilde{b})$ comply with **Eq. (28)**; hatched lines are the unstable regions for solutions of **Eq. (28)**.

Thus the general bifurcation problem contained in the arriving at a solution $\Delta T(t)$ is reduced to the determination of the solution set of Eq. (22) for the appropriate joint trajectory $\{\tilde{a}(t), \tilde{b}(t)\}$ in the space of controlling parameters (Fig. 12).

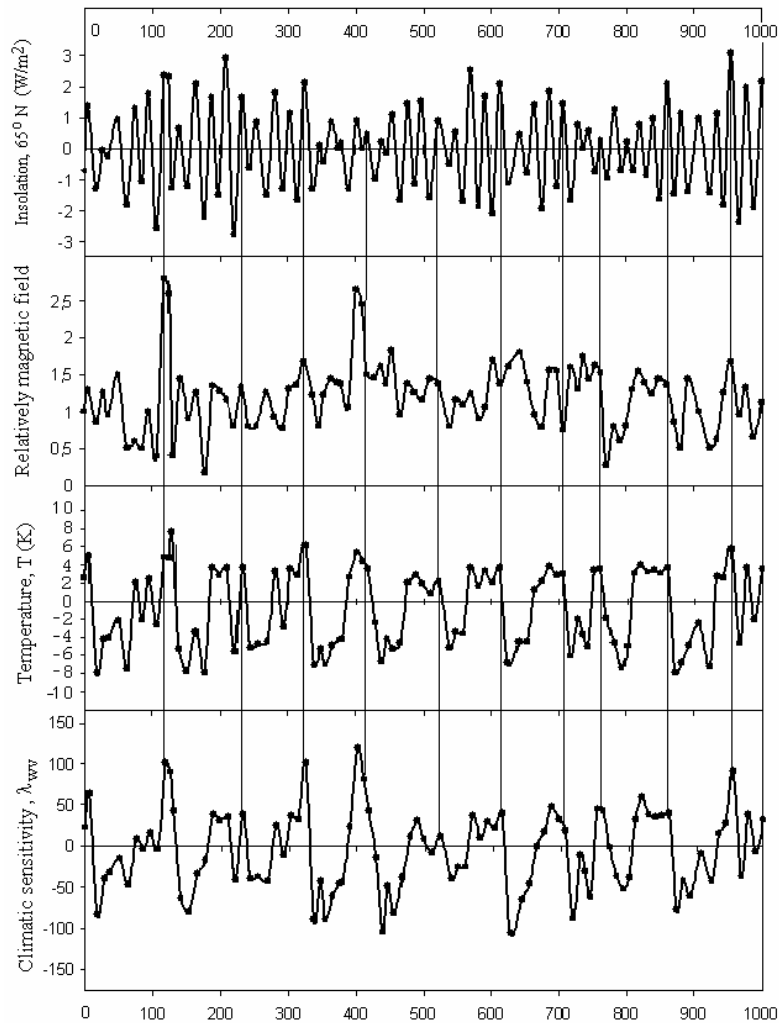
$$\lambda_{w+v} = \frac{1}{\varepsilon_{w+v} \Delta t} \cdot \frac{d}{d(\Delta T)} \Delta G_{w+v}(\Delta T, t) =$$

$$= \frac{1}{\Delta t} \frac{d(\Delta m_{w+v})}{d(\Delta T)} = \frac{1}{\varepsilon_{w+v} \Delta t} \left(\tilde{a}_0 \Delta T + \tilde{b}_0 \frac{4}{\eta_\alpha} \frac{2a_\mu T_0 + b_\mu}{\sigma_S} \right) M_\oplus^*(t), \quad (38)$$

where $\varepsilon_{w+v} \approx \varepsilon_w \approx \varepsilon_v$, i.e. it is supposed that the mean radiant powers of water vapour and liquid water are equal, $\Delta t = 10 \text{ kyr}$ – time scale resolution .



Numerical experiment



Model of climatic response insolation and magnetic field variations of the past 730 kyr compared with isotopic temperature data on climate of the past 420 kyr. Variations in orbital eccentricity (*a*) and insolation (*b*) at 65°N at the summer solstice over the past 730 kyr [Berger, 1978]. Variations of magnetic paleointensity (*c*) over the past 730 kyr [Yamasaki and Oda, 2002] and adapted data (*d*) of magnetic paleointensity (*c*). Vostok time series of isotopic temperature ΔT_S (*e*) at the surface [Petit et al., 1999] and result of our model calculated (*f*) by Eq. (28): evolution of the increment of temperature ΔT relative to the average temperature $T_0=286.6$ K over the past 730 kyr. Any underestimates of temperature changes ΔT_S (*e*) are defined by underestimates in the design formulae (*e*), where ΔT_1 is the temperature at the atmospheric (inversion) level, $\Delta \delta D_{\text{ice}}$ and $\Delta \delta^{18}\text{O}_{\text{sw}}$ is the globally averaged change from today's value of isotopic content of snow δD_{ice} and seawater $\delta^{18}\text{O}$ respectively. Dotted line (*f*) is the solution of bifurcation equation (28) under fixed magnetic field ($M_{\otimes}^n(t) \equiv 2$).

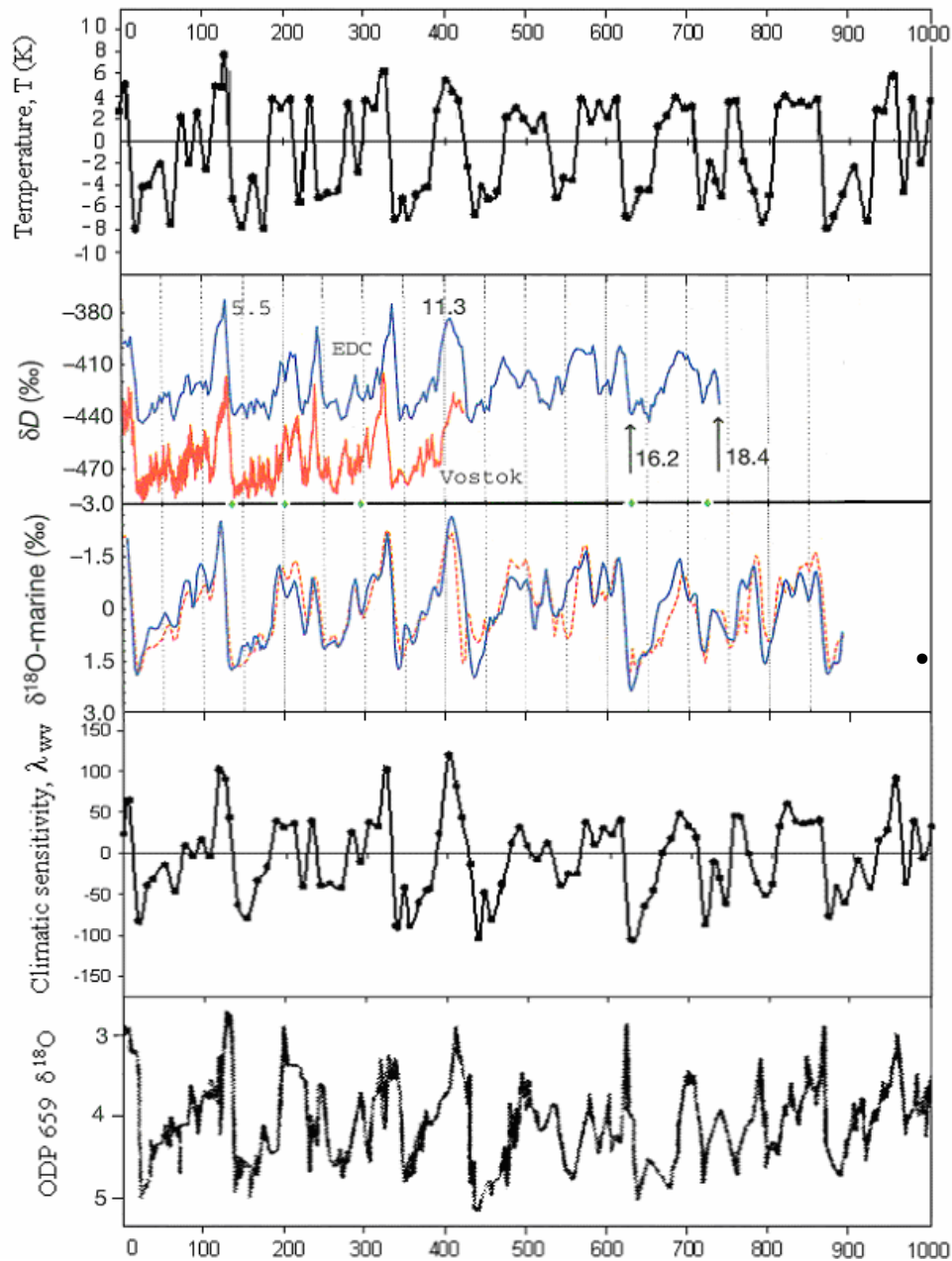


Fig.13. Comparison of time series of seawater $\delta^{18}O$ (ice volume proxy) from (a) *Bassinot et al.* [36] and (c) *Tidemann et al.* [37] with time series (b) of climatic sensitivity λ_{w+v} (ice volume proxy) calculated by Eq. (38).

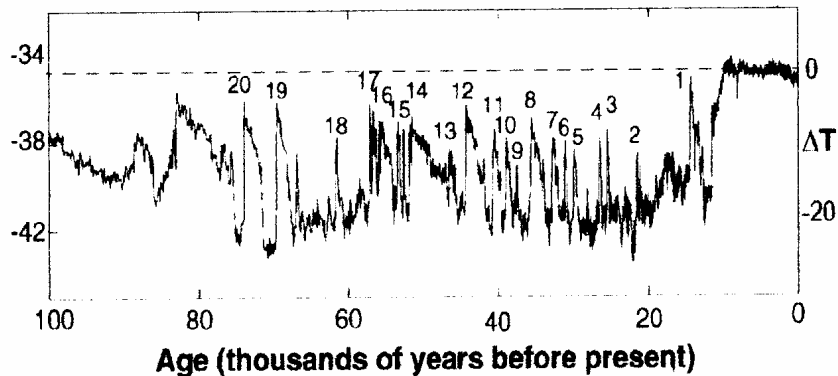
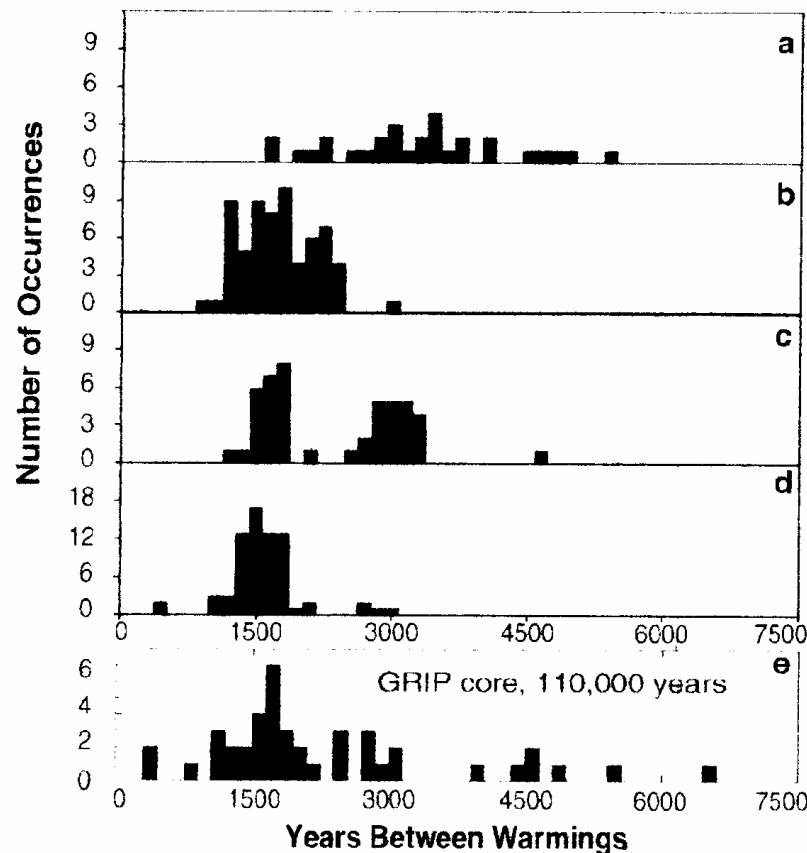


FIG. 1. Record of $\delta^{18}\text{O}$ [per mille (0.1%), scale on left] from the GRIP ice core, a proxy for atmospheric temperature over Greenland (approximate temperature range [3], in $^{\circ}\text{C}$ relative to Holocene average, is given on the right). Note the relatively stable Holocene climate during the past 10 kyr, and before that the much colder glacial climate punctuated by Dansgaard-Oeschger warm events (numbered).

FIG. 4. Interspike interval distribution (or waiting time between warm events) for “noise only” experiments (a),(b) and “noise plus signal” [(c),(d); amplitude = 0.01 Sv]. Standard deviation of the noise is $\sigma_F = 0.035$ Sv in panels (a),(c) and $\sigma_F = 0.05$ Sv in panels (b),(d). Each distribution was obtained from a simulation of 110 000 climate years. The bottom panel (e) is from the equally long Greenland ice core record and is taken from [4].



$$\Delta U(\Delta T, t) = \frac{1}{4} \Delta T^4 - \frac{1}{2} \tilde{a}_{DO} \Delta T^2 - \tilde{b}_{DO} \Delta T, \quad \text{where } \tilde{a}_{DO}, \tilde{b}_{DO} > 0 \quad (40)$$

Здесь следует напомнить, что усреднение изотопных данных в NGRIP-record производилось с учетом high time scale resolution, которое составило $\Delta t = 50 \text{ yr}$ [41]. А это означает, что в силу известного спектра колебаний температуры воздуха в Северо-Атлантическом секторе земного шара по Куцбаху и Брисону [16], в этом временном интервале ЗКС будет преобладать спектр колебаний стохастического климата, характеризуемого смесью белого шума и $1/f$ – шума (рис.3). Учитывая, что SR in a bistable potential is fully characterized as a synchronization effect of the hopping mechanism induced by the external periodic bias, например, слабым гармоническим сигналом $A \sin \omega t$, *for overdamped system the dependence $\Delta T(t)$ is to be found from*

$$\dot{x} = -\partial(\Delta U^*)_x(x, t) + A \sin \omega t + \zeta(t), \quad x(t) \equiv \Delta T(t) \quad (41)$$

или

$$\dot{x} = \tilde{a}_{DO} x - x^3 + \tilde{b}_{DO} + A \sin \omega t + \zeta(t) \quad (42)$$

где \dot{x} – температурное “трение” ЗКС о стенки потенциальной ямы, $\zeta(t) = \xi(t) + \eta(t)$ – аддитивная смесь белого шума и $1/f$ – шума соответственно.

where W_K and τ_K is the modified Kramer's rate и Kramer's time соответственно [38], характеризующие скорость и время переходов возбужденной системы через потенциальный барьер в условиях слабого периодического возмущения.

Очевидно, что из-за отсутствия периодической компоненты в (45), при построении функции the residence-time distribution (44) будут наблюдаться a series of peaks, centered of odd multiples of the half driving period

$$T_n \cong (2n + 1) \frac{\pi}{\omega} = (2n + 1) \frac{T_\omega}{2}, \quad n = 0, 1, \dots \quad (46)$$

где ω и T_ω – соответственно частота и период внешнего периодического возмущения. Более того, из анализа выражения (45) следует, что пики (46) появляются только при включении слабого гармонического возмущения, в обратном случае наблюдается монотонный экспоненциальный спад функции (44). Таким образом, физическая интерпретация (44) достаточно наглядна и заключается в том, что экспоненциальный фон представляет собой ту часть функции residence-time distribution (44), которая генерируется переключениями, вызванными только шумом, тогда как пики (46) есть отражение синхронизации между механизмами вылета и внешним периодическим возмущением.

At large noise, the term $-\tilde{b}_{DO} x$ causing the asymmetry in (39) и (40) can be neglected. Принимая во внимание этот факт и одновременно то, что по данным вычислительного эксперимента по моделированию abrupt glacial climate changes due to SR [40] применялся только белый шум $\xi(t)$, перепишем уравнение (42) с учетом этих условий:

$$\dot{x} = \tilde{a}_{DO} x - x^3 + A \sin \omega t + \xi(t), \quad x(t) \equiv \Delta T(t) \quad (43)$$

где амплитуда слабого внешнего периодического сигнала A ограничена weak-forcing limit $Ax_m \ll \Delta(\Delta U^*(x,t)) = \Delta U^*(0) - \Delta U^*(x_m)$. Here, $\pm x_m = (\tilde{a}_{DO})^{1/2}$ denote the potential minima and $\Delta(\Delta U^*(x,t)) = \tilde{a}_{DO}^2/4$ the potential barrier, $\xi(t)$ is a white Gaussian zero-mean-valid noise with correlation function $\langle \xi(t), \xi(0) \rangle = 2D\delta(t)$. В большинстве случаев, идентифицировать эффект SR удобнее с помощью экспериментального исследования статистики the residence-time исследуемой системы в потенциальной яме или, точнее говоря, с помощью так называемого the residence-time distribution [42]

$$P(t) \sim \exp(-W_K t)$$

$$W_K = \frac{1}{\tau_K} = \frac{1}{2\pi} \left[\left. \frac{d^2 \Delta U^*}{dx^2} \right|_{x=0} \left. \frac{d^2 U^*}{dx^2} \right|_{x=x_m} \right]^{1/2} \exp \left(- \frac{\Delta U^* \Big|_{x=0} - \Delta U^* \Big|_{x=x_m} + x_m A \sin \omega t}{D} \right) \quad (44)$$

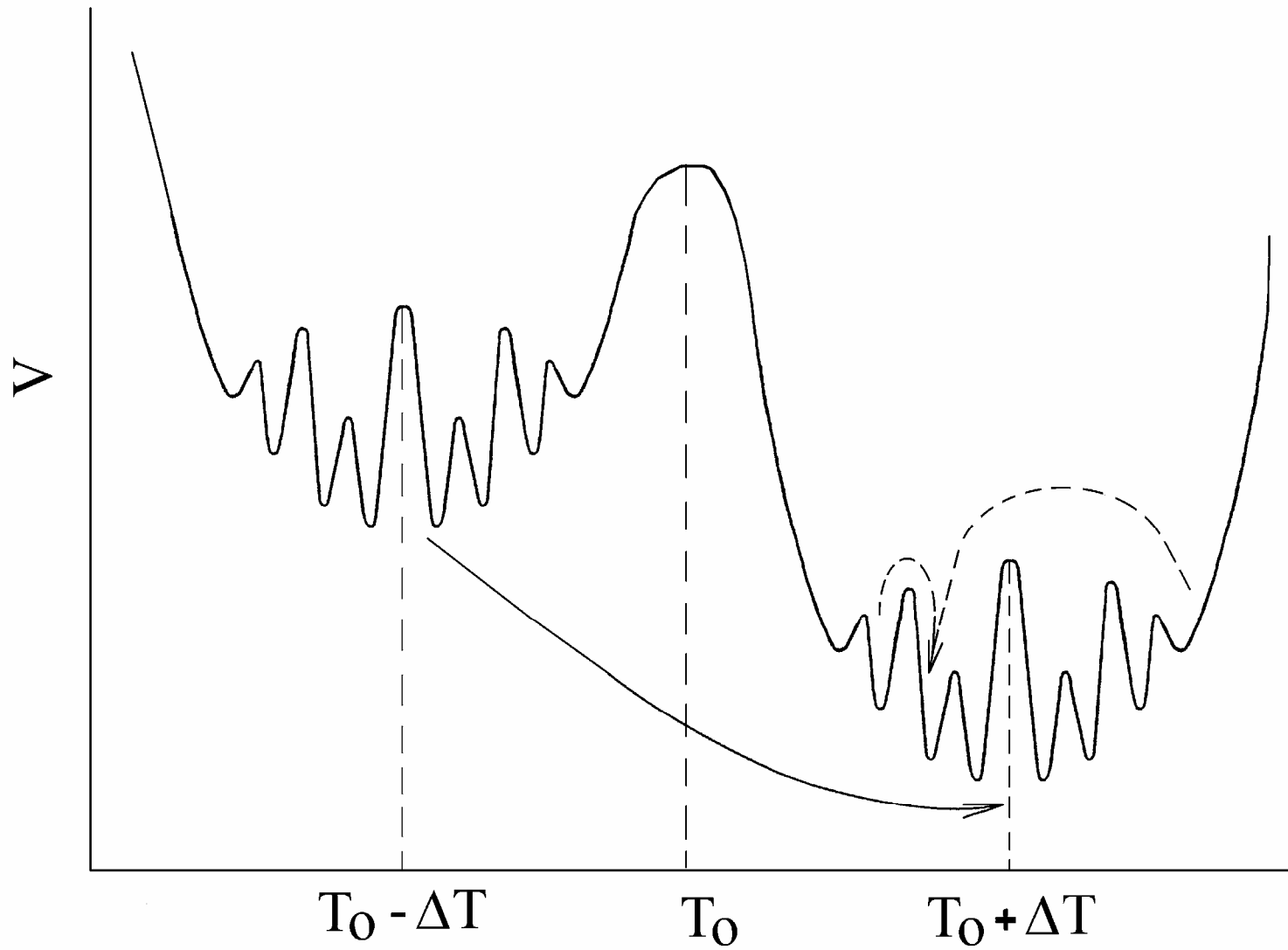
Именно использование идеологии оптимальной синхронизации при моделировании уравнения стохастического резонанса типа (43) в рамках бистабильного варианта climate model позволило авторам работы [40] построить “экспериментальную” функцию the residence-time distribution. При этом оказалось, что свойства the modeled warm events, с помощью которых было получено the residence-time distribution, находились в хорошем согласии с реальными свойствами of the Dansgaard-Oeschger events recorded in Greenland ice and other climate archives [40].

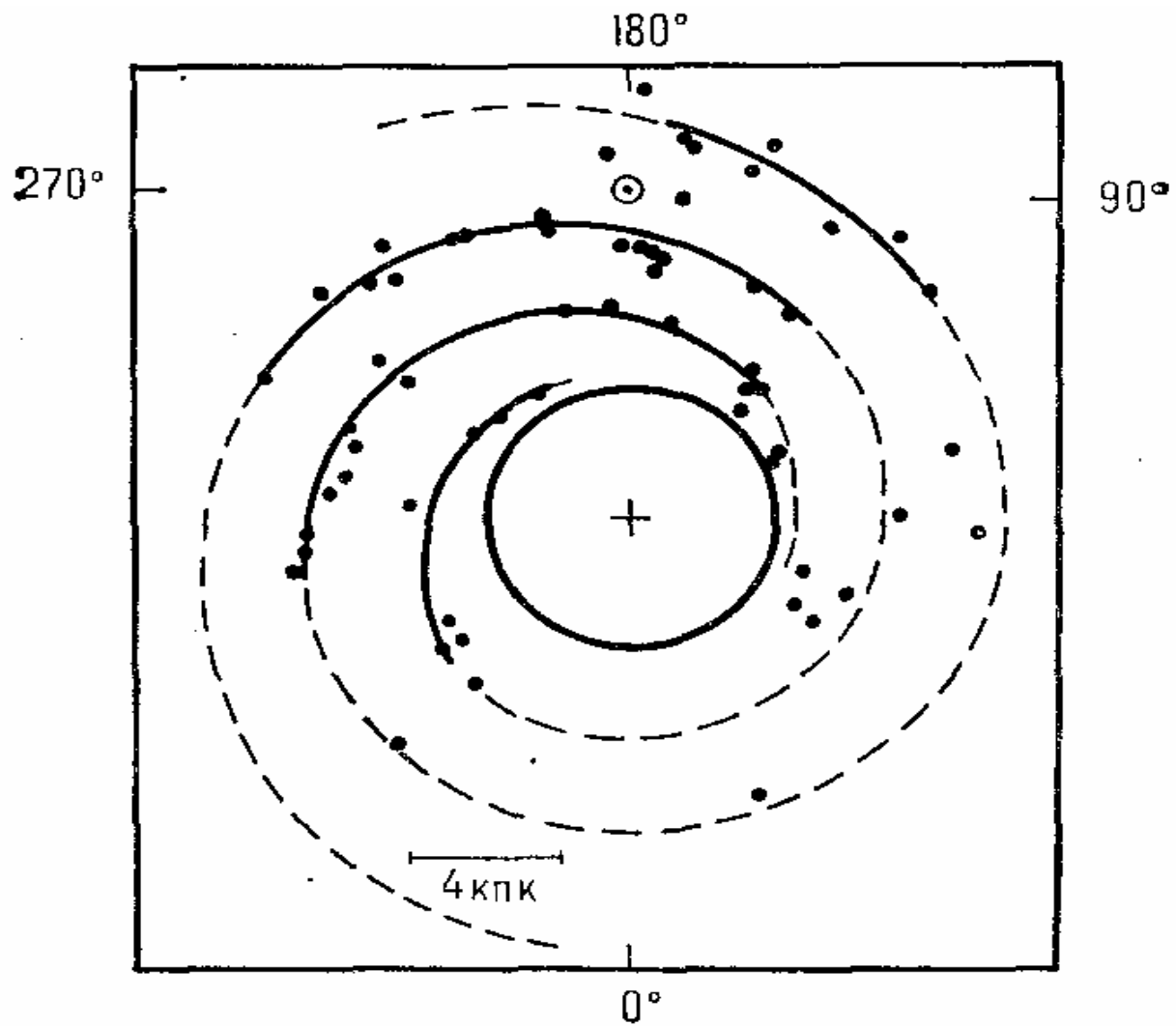
И, наконец, приведем краткий комментарий к так называемой проблеме “doubling CO₂”. Простой анализ структурных членов time-dependent управляющего параметра $\tilde{b}(t)$ указывает на то, что он содержит в себе три независимые компоненты (см. (26)): вариации инсоляции $\Delta\hat{S}(t)$ и radiation forcing of total mass water (vapour and liquid) в атмосфере $\Delta\hat{\mathcal{R}}_{w+v}M_{\oplus}^*(t)$ а также климатическую константу $\Delta\hat{\mathcal{R}}_{CO_2}$ характеризующую степень изменения дифференциальной radiation forcing of CO₂. При этом с помощью (26) нетрудно показать, что для любого $t=0\div 730 kyr$ практически всегда (за редким исключением (см. рис.7f) выполняется следующее неравенство:

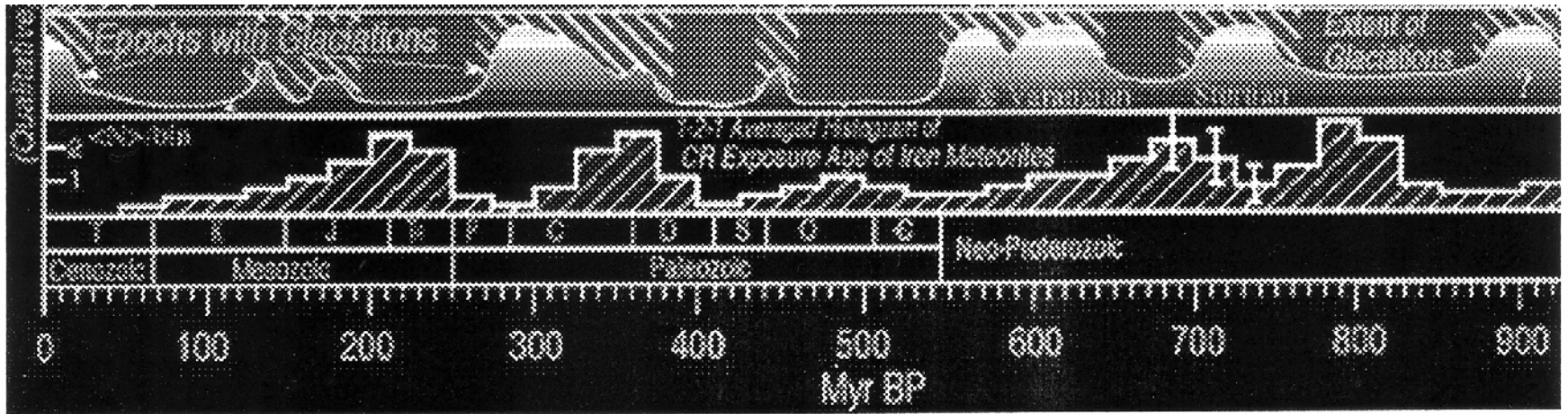
$$\Delta\hat{\mathcal{R}}_{CO_2} \ll \left| \frac{\eta_{\alpha}}{4} \Delta\hat{S}(t) + \Delta\hat{\mathcal{R}}_{w+v}M_{\oplus}^*(t) \right|, \quad for \quad \forall t \in [0, 730kyr] \quad (47)$$

Неравенство (47) означает тот факт, что существенное влияние anthropogenic perturbation возможно только в случае значительного увеличение вклада дифференциальной мощности тепловой энергии $(\Delta\hat{\mathcal{R}}_{CO_2})_{perturb}$ переизлучаемой углекислым газом, по сравнению с present-day $\Delta\hat{\mathcal{R}}_{CO_2}$. Например, с помощью очевидной модификации (37) нетрудно с помощью вычислительного эксперимента на основе (28) и/или (38) показать, что на интервале $t=0\div 120 kyr$ пороговый anthropogenic тепловой эффект наступает примерно при 15-кратном увеличении present-day $\Delta\hat{\mathcal{R}}_{CO_2}$ (точечная кривая на рис.8b). Другими словами, в рамках обсуждаемой бифуркационной модели глобального климата Земли так называемой anthropogenic проблемы “doubling CO_2 ” практически не существует.

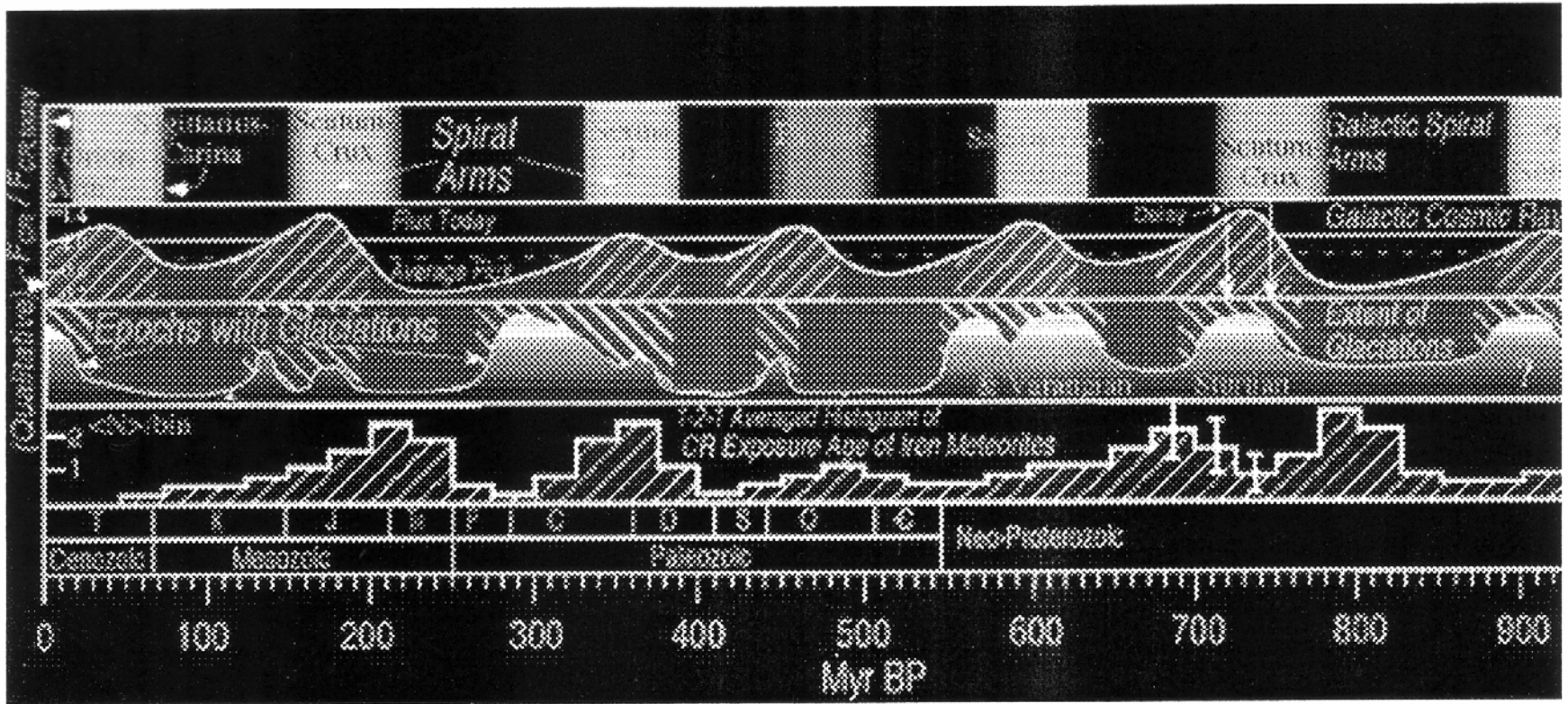
Подводя заключительные итоги, можно сказать, что самым важным, по нашему мнению, утверждением настоящей модели является то, что глобальный климат Земли, с одной стороны, полностью определяется двумя управляющими параметрами – инсоляцией и galactic cosmic rays, а с другой – при наличии теоретических или экспериментальных значений long-term variations of relative paleointensity $M_{\oplus}^*(t)$ практически не имеет ограничений на горизонт глобального прогноза on millennial time scale, т.е. вполне предсказуем.







The top panel describes our passages through galactic spiral arms. The second panel describes the predicted cosmic ray flux and the predicted occurrence of ice-age epochs. The third panel describes the actual occurrence of ice-age epochs. The fourth panel indirectly describes the variable cosmic ray flux. Due to the fact that the cosmic ray flux is the "clock" used to exposure date meteorites, the meteoritic ages are predicted to cluster around



The top panel describes our passages through galactic spiral arms. The second panel describes the predicted cosmic ray flux and the predicted occurrence of ice-age epochs. The third panel describes the actual occurrence of ice-age epochs. The fourth panel indirectly describes the variable cosmic ray flux. Due to the fact that the cosmic ray flux is the "clock" used to exposure date meteorites, the meteoritic ages are predicted to cluster around

Conclusions

It can be concluded from the above mentioned that the most important, in our opinion, statement of presented model is the fact that the Earth climate, on the one hand, is completely defined by the two controlling parameters – insolation and galactic cosmic rays – and, in the other hand, is quite predictable on the millennial time scales if only theoretical or experimental values on long-term variations of relative of relative paleointensity $M_{\oplus}^*(t)$ are present.

